Biodegradable Poly(butylene succinate-*co*-butylene adipate)/Multiwalled Carbon Nanotube Nanocomposites: Preparation, Morphology, and Crystallization Behavior

Siyu Zhu, Yuanyuan Zhao, Zhaobin Qiu

State Key Laboratory of Chemical Resource Engineering, Key Laboratory of Carbon Fiber and Functional Polymers, Ministry of Education, Beijing University of Chemical Technology, Beijing 100029, China

Received 13 April 2011; accepted 2 August 2011
DOI 10.1002/app.35407
Published online 29 November 2011 in Wiley Online Library (wileyonlinelibrary.com).

ABSTRACT: Biodegradable poly(butylene succinate-*co*-butylene adipate) (PBSA)/multiwalled carbon nanotubes (MWCNTs) nanocomposites were prepared via a simple melt-compounding method at low MWCNTs contents. Scanning and transmission electron microscopy observations revealed a relatively nice dispersion of MWCNTs throughout the PBSA matrix. Both the nonisothermal and isothermal melt crystallizations of PBSA were enhanced significantly in the nanocomposites relative to neat PBSA because of the presence of MWCNTs; however, the crystal structure of PBSA remained unchanged. © 2011 Wiley Periodicals, Inc. J Appl Polym Sci 124: 4268–4273, 2012

Key words: biodegradable; crystallization; nanocomposites

INTRODUCTION

Biodegradable poly(butylene succinate-*co*-butylene adipate) (PBSA), a copolymer of poly(butylene succinate), has received more attention recently.[1–3] Relative to poly(butylene succinate), PBSA is very susceptible to biodegradation because of its lower crystallinity and more flexible polymer chains. Carbon nanotubes (CNTs) were first reported by Iijima in 1991;[4] they possess excellent mechanical, electrical, and thermal properties. Some polymer/CNTs nanocomposites have been reported in the literature.[5–8] It is clear that the combination of biodegradable polymers with a very small quantity of CNTs is of great interest and use from both academic and industrial viewpoints.[9–19]

It should be noted that the fine dispersion of CNTs in the polymer matrix is of great importance for the preparation of high-performance polymer/CNTs nanocomposites. To avoid the serious aggregation of CNTs in the polymer matrix, the following three factors are very important: (1) including the use of CNTs containing functional groups, such as carboxyl groups, (2) the preparation of polymer/CNTs nanocomposites via solution casting with sonication or the *in situ* polymerization method, and (3) a lower CNTs content. However, melt compounding is the simplest method for fabricating high-performance polymer nanocomposites at low cost, although it may be less effective for dispersing CNTs in the polymer matrix.[5,11,20]

In this study, we prepared PBSA/pristine multiwalled carbon nanotube (MWCNTs) nanocomposites at 0.5 and 1 wt % MWCNTs contents via a simple melt-compounding method using a melting mixer at a relatively high rotor speed to get a fine dispersion of MWCNTs in the PBSA matrix; moreover, the effects of the MWCNTs on the crystallization behavior and crystal structure of PBSA were investigated.

EXPERIMENTAL

Materials and preparation of the PBSA/MWCNTs nanocomposites

PBSA (weight-average molecular weight = 3.77×10^4 g/mol) was obtained from Showa High Polymer Co., Ltd. (Japan). Pristine MWCNTs (purity > 95%) were purchased from Chengdu Institute of Organic Chemistry, Chinese Academy of Sciences (Chengdu, China). The diameter was around 30–50 nm with lengths ranging between 10 and 20 μm. The PBSA/MWCNTs nanocomposites containing 0.5 and 1 wt % MWCNTs were prepared via a melt-compounding method with a melting mixer (MS-II; Beihang University) at 105°C for 15 min with a high rotor speed of 150 rpm. In this work, neat PBSA and the PBSA/MWCNTs nanocomposites were abbreviated as 100/0, 99.5/0.5, and 99/1, respectively, with the

Correspondence to: Z. Qiu (qiuzb@mail.buct.edu.cn).
Contract grant sponsor: National Natural Science Foundation, China; contract grant number: 20974012.

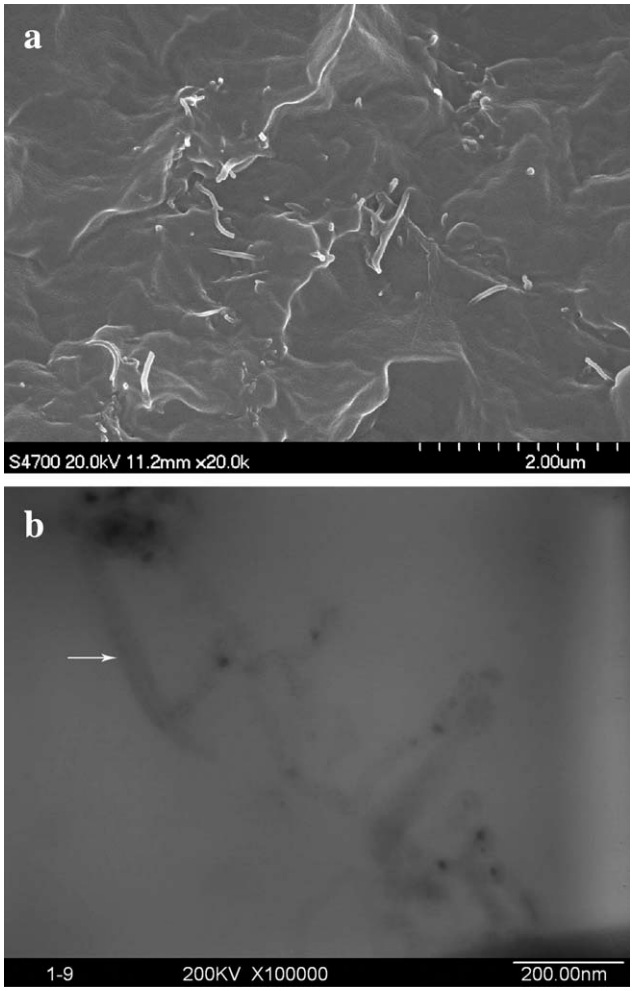

Figure 1 Dispersion of the MWCNTs in the PBSA matrix: (a) SEM and (b) TEM images.

first number referring to the percentage of PBSA and the second number referring to the percentage of MWCNTs.

Characterizations

A field emission scanning electron microscope (SEM) (S-4700, Hitachi Co., Tokyo, Japan) was used to observe the morphology of the surfaces of the PBSA/MWCNTs nanocomposites fractured in liquid nitrogen. The sample was coated with gold before examination.

A transmission electron microscope (H-800, Hitachi Co.) was also used to investigate the dispersion of MWCNTs in the PBSA matrix under an accelerating voltage of 200 kV. The nanocomposite specimen for the transmission electron microscopy (TEM) observation was about 50–70 nm thick; the specimen was prepared by ultramicrotoming under cryogenic conditions with a Leica ultramicrotome (Leica EM FC 6) with a diamond knife.

Thermal analysis was carried out with a TA Instruments differential scanning calorimeter (DSC) (Q100) (New Castle, Delaware) with a Universal Analysis 2000. All operations were performed under nitrogen purge, and the weight of the samples varying between 4 and 5 mg. Two different procedures, that is, nonisothermal melt crystallization and isothermal melt crystallization, were employed to study the crystallization behavior of neat PBSA and its nanocomposites. For nonisothermal melt crystallization, the samples were first heated to 130°C at 40°C/min, held at 130°C for 3 min to erase any thermal history, and then cooled to −10°C at different constant cooling rates ranging from 2.5 to 12.5°C/min. The crystallization peak temperature (T_p) was obtained from the cooling traces. For isothermal melt crystallization, the samples were annealed at 130°C for 3 min to erase any thermal history, cooled to the desired crystallization temperature (T_c) at 40°C/min, and then maintained at T_c until the crystallization was complete. The exothermal traces were recorded for later data analysis.

The spherulitic morphologies of the neat PBSA and the PBSA/MWCNTs nanocomposites were observed with polarizing optical microscopy (POM; Olympus BX51) (Tokyo, Japan) with a temperature controller (Linkam THMS 600). The samples were first annealed at 130°C for 3 min to erase any thermal history and then cooled to 80°C at 40°C/min.

Wide-angle X-ray diffraction (WAXD) patterns were recorded with a Rigaku D/Max 2500 VB2t/PC X-ray diffractometer (Tokyo, Japan) from 10 to 40° at 3°/min. The Cu Kα radiation source ($\lambda = 0.15418$ nm) was operated at 40 kV and 200 mA. The samples were first pressed into films with a thickness of around 0.5 mm on a hot stage at 130°C and then transferred into a vacuum oven at 80°C for 24 h.

RESULTS AND DISCUSSION

Morphology and dispersion of the MWCNTs in the PBSA matrix

The nice dispersion of CNTs in the matrix is one of the most important factors for improving the mechanical, electrical, and thermal performances of a polymer matrix; therefore, the dispersion of MWCNTs in the PBSA matrix was investigated with SEM and TEM first. Figure 1(a) shows an overview of the fracture surface of the 99/1 nanocomposite (abbreviated as 99/1 hereafter) as an example. As shown in Figure 1(a), the bright dots and lines are the ends of the broken CNTs and are indicative of a relatively nice dispersion of MWCNTs in the PBSA matrix. As shown in Figure 1(b), the MWCNTs remained curved in shape or even interwoven in the nanocomposite (as shown by the arrow) because of the extreme flexibility of the nanotubes. Both the SEM and TEM images revealed a fine dispersion of

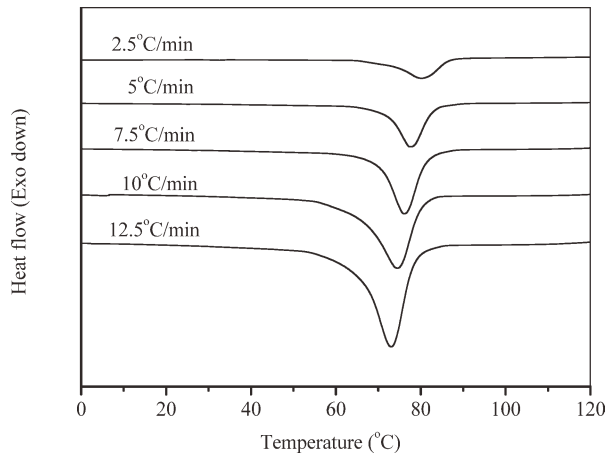

Figure 2 DSC traces of 99/1 cooled from the melt at various cooling rates ranging from 2.5 to 12.5°C/min.

MWCNTs in the PBSA matrix; this indicated that the PBSA/MWCNTs nanocomposites were successfully prepared without serious MWCNTs aggregation via a simple melt-compounding method at a relatively high rotor speed and lower MWCNTs contents.

Effect of the MWCNTs on the nonisothermal melt crystallization of PBSA in the PBSA/MWCNTs nanocomposites

The effect of MWCNTs on the crystallization behavior of PBSA was studied. The nonisothermal melt crystallization behaviors of neat PBSA and its nanocomposites were studied at various cooling rates from 2.5 to 12.5°C/min first. Figure 2 shows the DSC traces of 99/1 as an example. It is clear from Figure 2 that the crystallization exotherms shifted to a low-temperature range with increasing cooling rate because there was not enough time for the sample to crystallize at a high-temperature range at a high cooling rate. Figure 3 summarizes the variation of T_p with different cooling rates for both neat PBSA and its nanocomposites. It is clear from Figure 3 that T_p shifted to a low-temperature range with increasing cooling rate for both the neat PBSA and its nanocomposites. Meanwhile, the T_ps of PBSA in the nanocomposites were higher than that of neat PBSA for a given cooling rate; moreover, the T_ps shifted to a high-temperature range with increasing MWCNTs content in the nanocomposites. For example, in the case of neat PBSA, T_p was around 54.6°C at 10°C/min; however, in the case of the 99.5/0.5 and 99/1 nanocomposites, the T_ps shifted up to 71.2 and 74.5°C, respectively. It was obvious that the variation in T_p was around 16.6°C with increasing MWCNTs content from 0 to 0.5 wt %, but the increase was only around 3.3°C with further increases in the MWCNTs content from 0.5 to 1 wt %. Such results indicate that the nonisothermal melt crystallization of PBSA was enhanced significantly by the presence of MWCNTs, and the degree of enhancement in T_p was influenced by the MWCNTs contents because of the heterogeneous nucleation agent effect.[9–11]

Effect of the MWCNTs on the isothermal melt crystallization of PBSA in the PBSA/MWCNTs nanocomposites

The isothermal melt crystallization kinetics of neat PBSA and its nanocomposites were further investigated with DSC at different T_cs. On the basis of the exothermic curves of heat flow as a function of time, recorded in the Experimental section, the relative degree of crystallinity (X_t) at the crystallization time (t) could be calculated by the following equation:

$$X_t = \frac{\int_{t_o}^{t} \left(\frac{dH_c}{dt}\right) dt}{\int_{t_o}^{t_\infty} \left(\frac{dH_c}{dt}\right) dt} \quad (1)$$

where dH_c/dt is the rate of heat evolution and t_0 and t_∞ are the onset and end of the crystallization time, respectively. Figure 4(a,b) shows the development of X_t with t for both neat PBSA and 99/1 at different T_cs, respectively. t was prolonged with increasing T_c for both neat PBSA and 99/1; this indicated that the crystallization was slowed at high T_c because of low supercooling. Meanwhile, at a given T_c of 80°C, the crystallization finished within around 19.5 min for neat PBSA, whereas the crystallization finished within around 2.1 min for 99/1. It was obvious that the addition of MWCNTs enhanced the isothermal melt crystallization of PBSA significantly.

The well-known Avrami equation was used to analyze the overall isothermal crystallization kinetics of both neat PBSA and its nanocomposites. The Avrami equation is as follows:

$$1 - X_t = \exp(-kt^n) \quad (2)$$

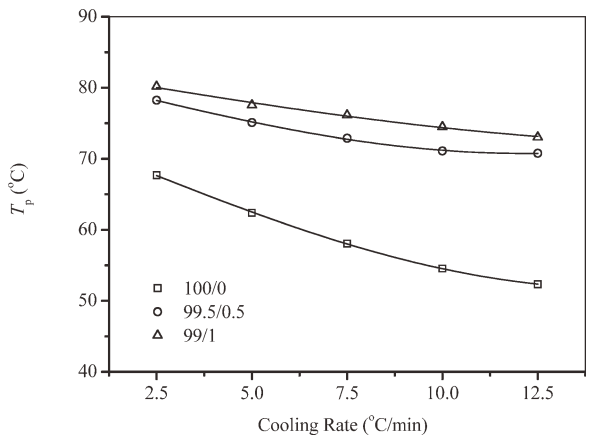

Figure 3 Variation of T_ps with cooling rates for neat PBSA and its nanocomposites.

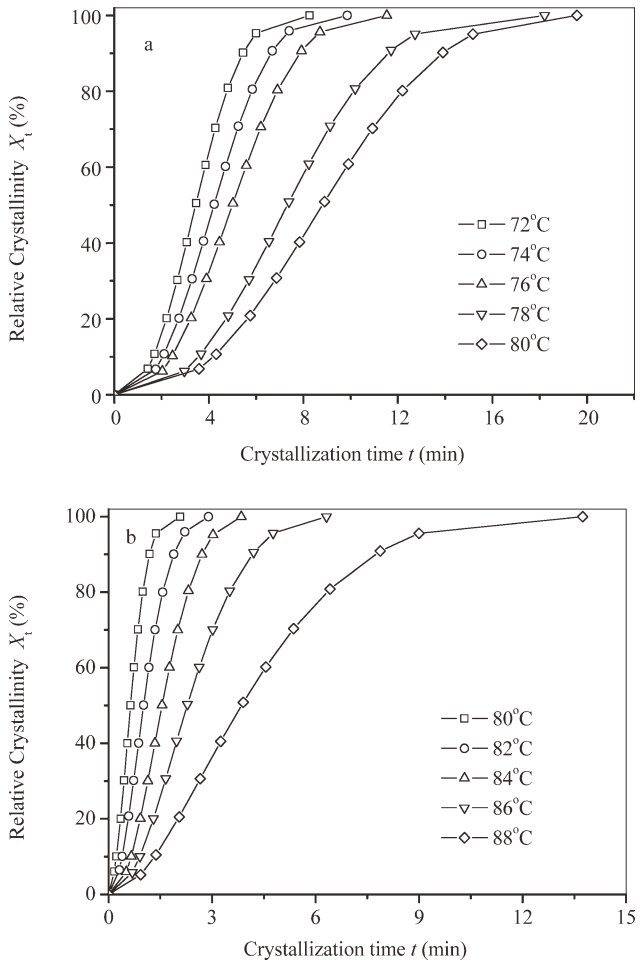

Figure 4 Development of X_t with t for (a) neat PBSA and (b) 99/1.

The equation was taken as double logarithms on both sides, as follows:

$$\log[-\ln(1 - X_t)] = n \log t + \log k \tag{3}$$

where X_t is the relative degree of crystallinity at time t, k is the crystallization rate constant, involving both nucleation and growth rate parameters, and n is the Avrami exponent and depends on the nature of nucleation and the growth geometry of the crystals.[21,22] Figure 5 shows the Avrami plots of neat PBSA and 99/1. It is clear from Figure 5 that the Avrami equation described the isothermal melt crystallization process very well because a serials of parallel lines were obtained. The values of n and k were obtained from the slopes and intercepts, respectively, of the Avrami plots. All of the related crystallization kinetics parameters are summarized in Table I for comparison. The value of n was 2.6 for neat PBSA; however, the value of n decreased to around 2.0 for 99.5/0.5 and 99/1. Such decrease in n was also found in nylon 66/MWNTs nanocomposites;[23] this suggests that the addition of MWCNTs decreased the growth dimension for the following two reasons. First, CNTs serve as one-dimensional templates (nuclei) from polymer crystal growth; therefore, the initial consumption of the polymer melt was one-dimensional in nature. Second, the growth of the polymer crystals is confined between the adjacent crystals because of the dense nucleation on the CNTs surfaces; this, thereby, decreases the dimension.[11]

However, it should be noted that it is difficult to compare the overall crystallization rate directly from the values of k because the unit of k is min^{-n} and n is not constant. Thus, the crystallization half-time ($t_{0.5}$), the time required to achieve 50% of the final crystallinity of the samples, is an important parameter for discussing the crystallization kinetics. The crystallization rate can usually be described by the reciprocal of $t_{0.5}$. The value of $t_{0.5}$ can be calculated by the following equation:

$$t_{0.5} = \left(\frac{\ln 2}{k}\right)^{1/n} \tag{4}$$

As shown in Table I, the values of $1/t_{0.5}$ decreased with increasing T_c for both neat PBSA and its nanocomposites, whereas those of $t_{0.5}$ increased with

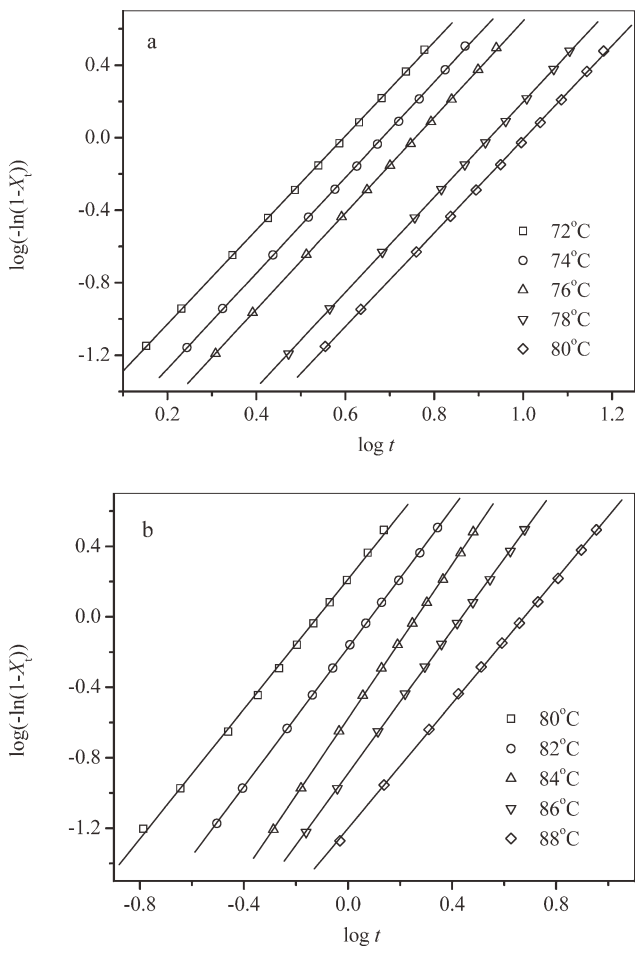

Figure 5 Avrami plots of (a) neat PBSA and (b) 99/1 at indicated T_cs.

TABLE I
Avrami Parameters for Neat PBSA and Its Nanocomposites

Sample	T_c (°C)	n	k (min^{-n})	$t_{0.5}$ (min)	$1/t_{0.5}$ (min^{-1})
Neat PBSA	72	2.6	2.84×10^{-2}	3.43	2.92×10^{-1}
	74	2.6	1.58×10^{-2}	4.20	2.38×10^{-1}
	76	2.6	9.89×10^{-3}	4.98	2.01×10^{-1}
	78	2.6	3.72×10^{-3}	7.31	1.37×10^{-1}
	80	2.6	2.57×10^{-3}	8.74	1.14×10^{-1}
PBSA/MWCNTs 99.5/0.5	78	2.1	1.26	7.51×10^{-1}	1.33
	80	2.1	5.74×10^{-1}	1.09	9.14×10^{-1}
	82	2.1	2.52×10^{-1}	1.63	6.12×10^{-1}
	84	2.0	1.08×10^{-1}	2.52	3.97×10^{-1}
	86	1.9	4.32×10^{-2}	4.15	2.41×10^{-1}
PBSA/MWCNTs 99/1	80	1.8	1.63	6.27×10^{-1}	1.59
	82	2.0	6.69×10^{-1}	1.02	9.82×10^{-1}
	84	2.2	2.65×10^{-1}	1.55	6.44×10^{-1}
	86	2.0	1.29×10^{-1}	2.29	4.38×10^{-1}
	88	1.8	6.30×10^{-2}	3.87	2.58×10^{-1}

increasing T_c. Such variations suggest that the isothermal crystallization rate decreased with increasing T_c for both neat PBSA and its nanocomposites. Moreover, at a given T_c, such as 80°C, $1/t_{0.5}$ was greater in the nanocomposites than in neat PBSA, and the value of $1/t_{0.5}$ in 99/1 was higher than that in the 99.5/0.5 nanocomposite. Such results indicate again that the crystallization process of PBSA in the nanocomposites was accelerated gradually with increasing MWCNTs content because of the heterogeneous nucleation effect.

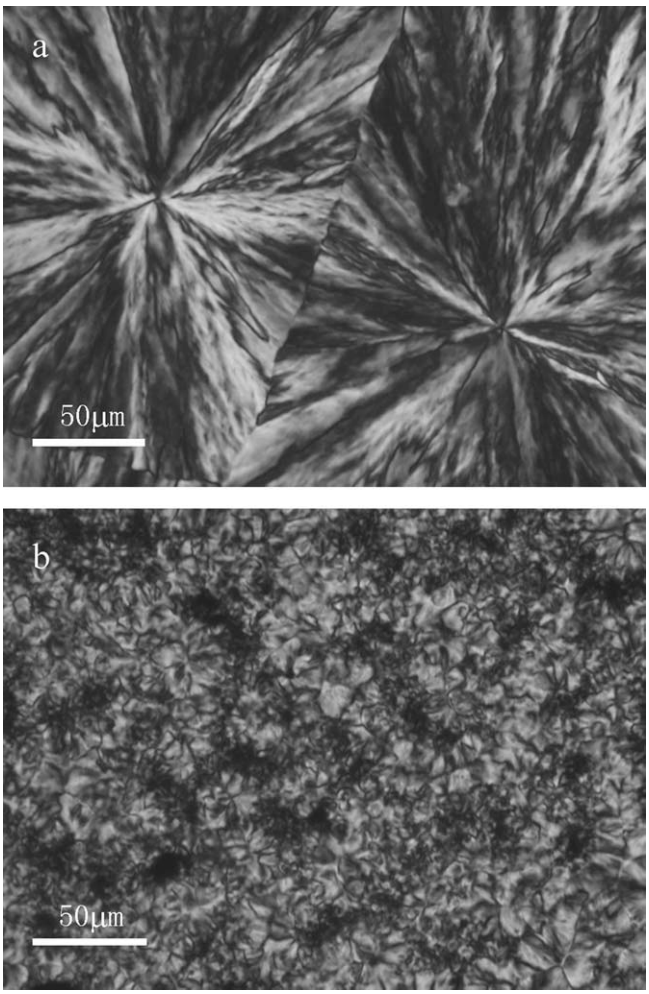

Figure 6 Optical micrographs (same magnification, bar = 50 μm) of the spherulitic morphology of neat PBSA and 99/1 after complete crystallization at 80°C: (a) neat PBSA and (b) 99/1.

Effect of the MWCNTs on the spherulitic morphology and crystal structure of PBSA in the PBSA/MWCNTs nanocomposites

The effect of the presence of MWCNTs on the spherulitic morphology of PBSA was studied with POM. Figure 6 shows the POM images of neat PBSA and 99/1 crystallized at 80°C. From Figure 6(a), it was found that the well-developed spherulites grew to a size of roughly several hundreds of micrometers in diameter in the case of neat PBSA. However, Figure 6(b) shows

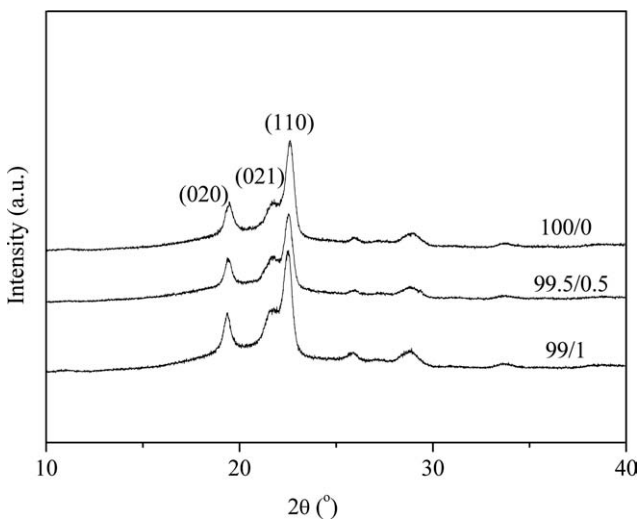

Figure 7 WAXD patterns of neat PBSA and its nanocomposites.

that the size of the PBSA spherulites became much smaller in the presence of MWCNTs; this was indicative of a heterogeneous nucleation effect of MWCNTs. On the basis of the POM study, it could be seen that the nucleation density of PBSA in 99/1 was higher than that of neat PBSA. Such results were consistent with the DSC results presented in the previous section. In brief, the presence of MWCNTs in the PBSA matrix had a significant influence on the spherulitic morphology and the overall crystallization process of PBSA in the nanocomposites.

It was of great interest to study the effect of MWCNTs on the crystal structure of PBSA. Figure 7 shows the WAXD patterns of neat PBSA and its nanocomposites after crystallization at 80°C for 24 h. As shown in Figure 7, both neat PBSA and its nanocomposites exhibited nearly the same diffraction peaks at almost the same locations; this indicated that incorporation with the MWCNTs did not modify the crystal structure of PBSA. The three main peaks located around 19.5, 21.7, and 22.6° were assigned to the (020), (021), and (110) planes of PBSA, respectively.[1]

CONCLUSIONS

Biodegradable PBSA/MWCNTs nanocomposites at low MWCNTs contents were prepared successfully through the simple melt-compounding method at a relatively high rotor speed in this work. Both the SEM and TEM observations revealed a relatively fine dispersion of MWCNTs throughout the PBSA matrix. The effects of MWCNTs on the nonisothermal melt crystallization, isothermal melt crystallization kinetics, and crystal structure of PBSA in the nanocomposites were investigated with DSC, POM, and WAXD in detail. The results show that both the nonisothermal and isothermal melt crystallizations of PBSA were enhanced by the presence of MWCNTs and that the degree of enhancement was influenced by the MWCNTs contents because of the heterogeneous nucleation effect. The isothermal melt crystallization kinetics of neat PBSA and its nanocomposites were successfully described by the Avrami method. The crystal structure of PBSA did not change, despite the presence of MWCNTs in the nanocomposites.

References

1. Qiu, Z.; Yan, C.; Lu, J.; Yang, W. Macromolecules 2007, 40, 5047.
2. Ray, S.; Bandyopadhyay, J.; Bousmina, M. Polym Degrad Stab 2007, 92, 802.
3. Ray, S.; Bandyopadhyay, J.; Bousmina, M. Eur Polym J 2008, 44, 3133.
4. Iijima, S. Nature 1991, 354, 56.
5. Liu, T.; Phang, I.; Shen, L.; Chow, S.; Zhang, W. Macromolecules 2004, 37, 7214.
6. Huang, S.; Wang, M.; Liu, T.; Zhang, W.; Tjiu, W.; He, C.; Lu, X. Polym Eng Sci 2009, 49, 1063.
7. Wang, S.; Shen, L.; Zhang, W.; Tong, Y. Biomacromolecules 2005, 6, 3067.
8. Gao, J.; Yan, D.; Huang, H.; Dai, K.; Li, Z. J Appl Polym Sci 2009, 114, 1002.
9. Qiu, Z.; Zhu, S.; Yang, W. J Nanosci Nanotechnol 2009, 9, 4961.
10. Zhao, Y.; Qiu, Z.; Yang, W. J Phys Chem B 2008, 112, 16461.
11. Ray, S.;Vaudreuil1, S.Maazouz, A.; Bousmina, M. J Nanosci Nanotechnol 2006, 6, 2191.
12. Hu, X.; An, H.; Li, Z.; Geng, Y.; Li, L.; Yang, C. Macromolecules 2009, 42, 3215.
13. Xu, J.; Chen, T.; Yang, C.; Li, Z.; Mao, Y.; Zeng, B.; Hsiao, B. Macromolecules 2010, 43, 5000.
14. Xu, H.; Dai, X.; Lamb, P.; Li, Z. J Polym Sci Part B: Polym Phys 2009, 47, 2341.
15. Ramontja, J.; Ray, S.; Pillai, S.; Luyt, A. Macromol Mater Eng 2009, 294, 839.
16. Song, L.; Qiu, Z. Polym Degrad Stab 2009, 94, 632.
17. Zhao, Y.; Qiu, Z.; Yang, W. Compos Sci Technol 2009, 69, 627.
18. Ko, S.; Hong, M.; Park, B.; Gupta, R.; Choi, H.; Bhattacharya, S. Polym Bull 2009, 63, 125.
19. Ko, S.; Gupta, R.; Bhattacharya, S.; Choi, H. Macromol Mater Eng 2010, 295, 320.
20. Moniruzzaman, M.; Winey, K. Macromolecules 2006, 39, 5194.
21. Avrami, M. J Chem Phys 1939, 8, 212.
22. Avrami, M. J Chem Phys 1941, 9, 177.
23. Li, L.; Li, C.; Ni, C.; Rong, L.; Hsiao, B. Polymer 2007, 48, 3452.